High-pressure phonon dispersion of copper by using the modified analytic embedded atom method*

Zhang Xiao-Jun(张晓军)[a)b)], Chen Chang-Le(陈长乐)[a)†], and Feng Fei-Long(凤飞龙)[b)]

[a)] *Shaanxi Key Laboratory of Condensed Matter Structures and Properties and Key Laboratory of Space Applied Physics and Chemistry, Ministry of Education, Northwestern Polytechnical University, Xi'an* 710072, *China*

[b)] *School of Science, Xi'an Polytechnic University, Xi'an* 710048, *China*

(Received 21 December 2012; revised manuscript received 21 April 2013)

By using the Born–von Kármán theory of lattice dynamics and the modified analytic embedded atom method, we reproduce the experimental results of the phonon dispersion in fcc metal Cu at zero pressure along three high symmetry directions and four off-symmetry directions, and then simulate the phonon dispersion curves of Cu at high pressures of 50, 100, and 150 GPa. The results show that the shapes of dispersion curves at high pressures are very similar to that at zero pressure. All the vibration frequencies of Cu in all vibration branches at high pressures are larger than the results at zero pressure, and increase correspondingly as pressure reaches 50, 100, and 150 GPa sequentially. Moreover, on the basis of phonon dispersion, we calculate the values of specific heat of Cu at different pressures. The prediction of thermodynamic quantities lays a significant foundation for guiding and judging experiments of thermodynamic properties of solids under high pressures.

Keywords: phonon dispersion, high pressure, simulation, modified analytic embedded atom method

PACS: 63.20.D−, 62.50.−p, 71.15.Pd, 12.39.Pn **DOI:** 10.1088/1674-1056/22/9/096301

1. Introduction

The phonon dispersion relation provides important information about many physical properties of a material such as specific heat, density of state, sound velocity and electron–phonon interaction related to the resistivity of metal, superconductivity, and the temperature dependence of optical spectrum.[1–3] In addition, low-frequency modes are closely associated with phase transformations under high pressure.[4,5] Recently, the phonon dispersion relations of a material at high pressures have been studied both experimentally and theoretically.[6–8] In the experimental aspect, the inelastic neutron scattering has been applied successfully to measure phonon dispersion curves of solids under high pressure.[6,9] Meanwhile, the static high-pressure experiment is experiencing a rebirth due to improved diamond-anvil techniques and extension to ultrasound and X-ray measurements under static pressures, where the applied static pressure is a continuously variable parameter which can be used for the study of the dynamical property of a solid as a function of the interatomic distance,[10] laying a crucial foundation for theoretically reproducing experiment results or predicting phonon dispersion curves under high pressure. Hong *et al.*[11] used density-functional theory (DFT) within quasi-harmonic approximation to describe the phonon spectra of Ir along symmetry directions under high pressures of 23.5 and 55 GPa. Hu *et al.*[12] reported on the phonon dispersion curves of Ti along four symmetry directions at different pressures using first-principles calculation. The aforementioned methods supply accurate information about the phonon dispersion relation. However, considerable computer power and time are required to obtain final results, especially for the phonon dispersion relation along off-symmetry directions at various pressures. In addition, computer limitations allow this method to simulate systems with only a few hundred atoms. For the above reasons, empirical many-body methods, for example, embedded atom method (EAM) proposed by Daw and Baskes,[13,14] have been developed to investigate physical properties of solids. The potential provides quick description in metallic systems. However, in the EAM, the bond angles are not considered in the expression of electron density. Based on the model, Ouyang *et al.*[15] and Zhang *et al.*[16] developed a modified analytic embedded atom method (MAEAM) to reflect exactly the interactions between atoms, by adding a modified term $M(P)$ to the total energy expression. The model was successful in calculating physical properties of materials such as interface,[17] grain boundary,[18] and vacancy diffusion.[19] So far, the MAEAM has not been used to calculate phonon dispersions under high pressures. Theoretical study of the phonon dispersion relation is of fundamental importance in comprehending underpinning physical mechanisms governing many properties of materials. In this paper, the MAEAM is used to simulate the phonon dispersions of copper (Cu) along symmetry directions and off-symmetry directions under high pressures of up to 150 GPa, and to test the validity of the MAEAM for lattice dynamics under high pressures.

*Project supported by the National Natural Science Foundation of China (Grant Nos. 61078057 and 11204227) and the Scientific Research Program of Education Department of Shaanxi Province, China (Grant No. 12JK0958).

†Corresponding author. E-mail: chenchl@nwpu.edu.cn

© 2013 Chinese Physical Society and IOP Publishing Ltd

2. Theoretical model and computational details

In the MAEAM, the total energy E_t of a system of atoms is expressed as[16,20]

$$E_t = \sum_i F(\rho_i) + \frac{1}{2}\sum_i \sum_{j\neq i} \phi(r_{ij}) + \sum_i M(P_i), \quad (1)$$

$$\rho_i = \sum_{j\neq i} f(r_{ij}), \quad (2)$$

$$P_i = \sum_{j\neq i} f^2(r_{ij}), \quad (3)$$

where $F(\rho_i)$ is the energy to embed an atom in site i with electron density ρ_i, which is given by a linear superposition of the spherically averaged atomic electron density of other atoms $f(r_{ij})$, r_{ij} is the separation distance from atom j to atom i, $\phi(r_{ij})$ is the interaction potential between atom i and atom j, and $M(P_i)$ is the modified term that describes the energy change due to the non-spherical distribution of electrons (P_i) and deviation from the linear superposition of atomic electronic density. The embedding function $F(\rho_i)$, pair potential $\phi(r_{ij})$, modified term $M(P_i)$, and atomic electron density $f(r_{ij})$ take the following forms:[21]

$$F(\rho_i) = -F_0[1 - n\ln(\rho_i/\rho_e)](\rho_i/\rho_e)^n, \quad (4)$$

$$\phi(r_{ij}) = k_0 + k_1(r_{ij}/r_{1e}) + k_2(r_{ij}/r_{1e})^2 + k_3(r_{ij}/r_{1e})^6 + k_4(r_{ij}/r_{1e})^{-12} + k_5(r_{ij}/r_{1e})^{-1}, \quad (5)$$

$$M(P_i) = \alpha\{1 - \exp[-(\ln|P_i/P_e|)^2]\}, \quad (6)$$

$$f(r_{ij}) = f_e(r_{1e}/r_{ij})^6, \quad (7)$$

where the subscript e indicates the equilibrium state, r_{1e} is the first nearest neighbor distance at equilibrium, and the electron density at equilibrium f_e is taken to be 1.[15] The remaining model parameters F_0, n, α, and k_i ($i = 0$–5) in the equations above can be determined by fitting lattice constant a, the cohesion energy E_c, mono-vacancy formation energy E_{1f}, and elastic constants C_{11}, C_{12}, and C_{44}. The calculated results are listed in Table 1.

Table 1. Calculated model parameters of Cu.

n	F_0/eV	α/eV	k_0/eV	k_1/eV	k_2/eV	k_3/eV	k_4/eV	k_5/eV
0.60	2.32	0.00316257	1.499487	−0.650171	0.097645	−0.000056	0.098837	−1.178326

Molecular dynamic (MD) simulation was carried out using a computer program compiled in MATLAB to obtain phonon dispersion curves of Cu within the framework of the lattice dynamics theory. In the simulation, an fcc cell is adopted, which is composed of a computational cell surrounded by a mantle of atoms at equilibrium positions. The computational cell is a $6a \times 6a \times 6a$ crystal with 1098 atoms, where a is the lattice constant. All the atoms are assumed to be arranged on the fcc lattice subjected to periodic boundary conditions in three dimensions. The interatomic interactions have been modelled with MAEAM, in which the potential functions are truncated at a cutoff distance of 6.26 Å. The pressure of the system is controlled by rescaling the atomic velocities at every two integration steps. The Verlet algorithm is used to integrate equations of motion in time step of 2 fs. More detailed expositions of numerical simulation method can be found in Refs. [22] and [23]. The relation of pressure–compress in the system is obtained from the equation of state (EOS) developed by Rose *et al.*[24] and Vinet *et al.*[25] According to the Rose–Vinet equation, the relation between pressure and compression can be expressed as

$$P = 3B_0(1-X)X^{-2}\exp[1.5(B_0' - 1)(1-X)], \quad (8)$$

where $X = (V/V_0)^{1/3}$, B_0 and B_0' are the bulk modulus and its pressure derivative at ambient pressure, and V_0 is the volume at ambient pressure. The P data are fitted with the Rose–Vinet formula of the EOS. The fitting results together with the available experimental data[26] are shown in Fig. 1.

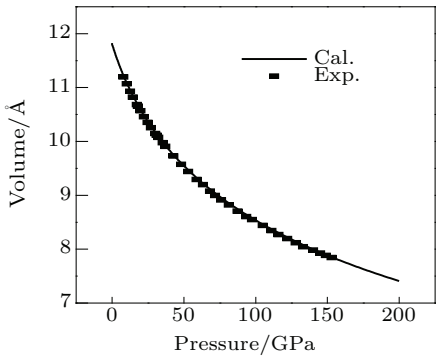


Fig. 1. Equation of state of Cu at ambient temperature. Solid squares: experimental values; solid line: fitting results.

3. Results and discussion

Within the harmonic approximation, dynamical matrices are computed based on the MAEAM to obtain phonons in the irreducible wedge of Brillouin zone (BZ). The phonon dispersion curves of Cu along high-symmetry directions [00ζ], [0$\zeta\zeta$], and [$\zeta\zeta\zeta$], as well as off-symmetry directions [0.5 1 − ζ ζ], [0.5 + ζ 1 − ζ 0], [0.5 + ζ 0.5 + ζ 0.5 − ζ], and [ζ 1 − ζ ζ] at zero pressure are shown in Figs. 2 and 3, respectively. The physical meanings of the notations in the figures can be found from Ref. [27]. According to the theory of lattice dynamics, the unit cell of fcc structure containing an atom can give rise to three phonon branches, which contain two transverse acoustic modes and one longitudinal acoustic mode. The two transverse acoustic modes merge usually into a vibration branch along [00ζ] and [$\zeta\zeta\zeta$] directions due to four- and six-fold rotation symmetry. As shown in Figs. 2 and 3, the exper-

imental results are basically consistent with the simulated results. The simulated phonon dispersions along high-symmetry directions are in general agreement with the experimental results obtained by Svensson *et al.*,[28] using thermal neutron inelastic scattering. There are some smaller deviations observed around some boundary points in the first Brillouin zone, such as X point in the L $[0\zeta\,\zeta]$ (that is, L branch in the $[0\zeta\,\zeta]$ direction) and T_2 $[0\zeta\,\zeta]$ branches (that is, L' point in the T $[\zeta\,\zeta\,\zeta]$ branch). It can be seen from Fig. 3 that along the off-symmetry directions, the dispersion curves have a shape very similar to the experimental results and the calculated phonon dispersions are substantially higher than the experimental values. The discrepancies may result from the fact that the current simulations are within harmonic approximation and adiabatic approximation, whereas, the measurements were obtained under conditions that the anharmonicity effects were not negligible. The effects of anharmonicity make each phonon frequency experience a shift.

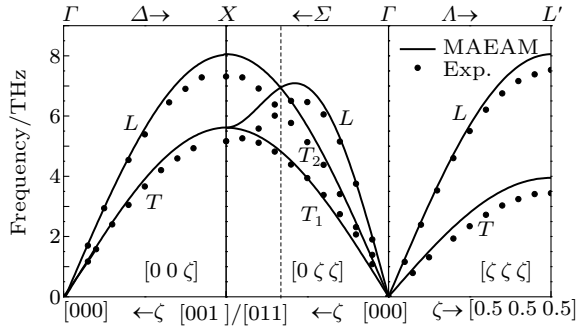


Fig. 2. Phonon dispersion curves of Cu at zero pressure along high-symmetry directions.

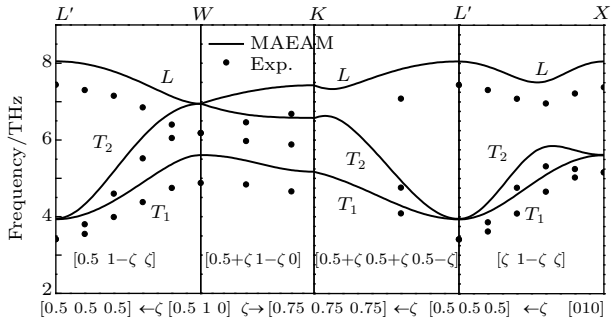


Fig. 3. Phonon dispersion curves of Cu at zero pressure along off-symmetry directions.

The phonon dispersion curves of Cu along high-symmetry directions under high pressures of 50, 100, and 150 GPa are shown in Fig. 4, where the dotted line represents the results at zero pressure for comparison. Four interesting features of the simulated dispersion curves at high pressures can be seen in Fig. 4. Firstly, the shapes of dispersion curves at 50, 100, and 150 GPa, respectively, are very similar to that at zero pressure at different phonon frequencies. The similarity among these dispersion curves is due to that metal Cu keeps its fcc structure till the maximum pressure studied (150 GPa). Secondly, the vibration frequencies of Cu in all vibration branches at pressures of 50, 100, and 150 GPa are larger than at zero pressure, and the frequencies increase with pressure as observed in fcc metals Ir and Cs.[11,29] The frequency of Cu at 50 GPa increases by 33% compared with that at 0 GPa. The frequency would increase by about 46% at 100 GPa and 52% at 150 GPa compared with that at 0 GPa. The variation is due to the volume compression resulting from force constants that are sensitive to pressure. Thirdly, a rather interesting aspect of the dispersion curves, namely, the anomalous dispersion, is exhibited in the T_1 $[0\zeta\,\zeta]$ branch at 150 GPa. The frequencies of the branches for ζ between approximately 0.4 and 0.8 are slightly above the velocity of sound. The anomalous phenomenon is present but obscure at 50 GPa and 100 GPa, and cannot be observed at zero pressure. To illustrate clearly the anomalous phenomenon, the vibration branches T_1 $[0\zeta\,\zeta]$ at zero pressure and 150 GPa are respectively plotted in Fig. 5, where the straight lines passing the point Γ represent the velocities of sound for the vibration branches. At long-wave limitation (at low frequency), the crystal can be treated suitably as a continuous medium, and the velocity of sound $\upsilon = \mathrm{d}\omega/\mathrm{d}k$ is the slop of vibration branch at low-ζ part. In general, the frequencies drop below the velocity of sound line (negative dispersion), like the T_1 $[0\zeta\,\zeta]$ branch at zero pressure. However, the frequencies of the branch T_1 $[0\zeta\,\zeta]$ for ζ between approximately 0.4 and 0.8 at 150 GPa are higher than the corresponding velocity of sound line (positive dispersion). The anomalous phenomenon may result from an electronic effect, namely, pressure induces a less effective electric shield from the vibrational motion of the nuclei. Fourthly, the gaps between L $[\zeta\,\zeta\,\zeta]$ branch and T $[\zeta\,\zeta\,\zeta]$ branch at high pressures become gradually wider as pressure reaches 0, 50, 100, and 150 GPa sequentially. In addition, we calculate the phonon spectra of Cu along off-symmetry directions under high pressures of 50, 100, and 150 GPa. As shown in Fig. 6, the curves exhibit shapes similar to the results at zero pressure, and the phonon frequencies for all considered branches in metal Cu also increase with increasing pressure.

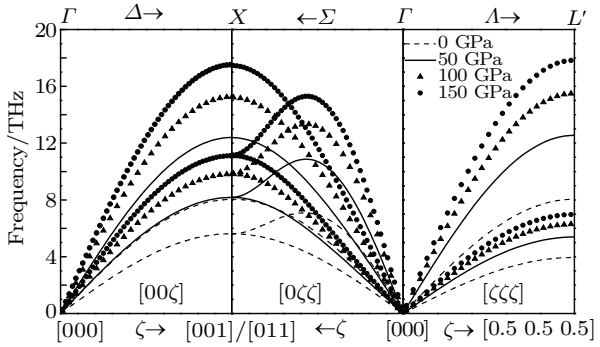


Fig. 4. Phonon dispersion curves of Cu along high-symmetry directions at different pressures.

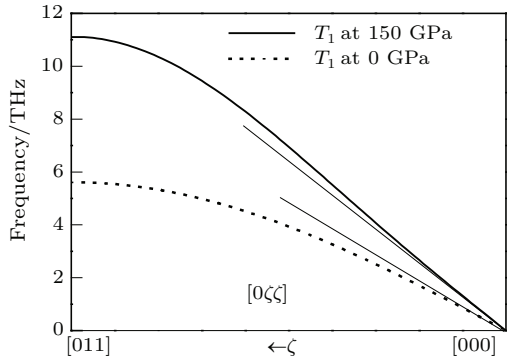


Fig. 5. Vibration branches T_1 $[0\zeta\,\zeta]$ at zero pressure and 150 GPa.

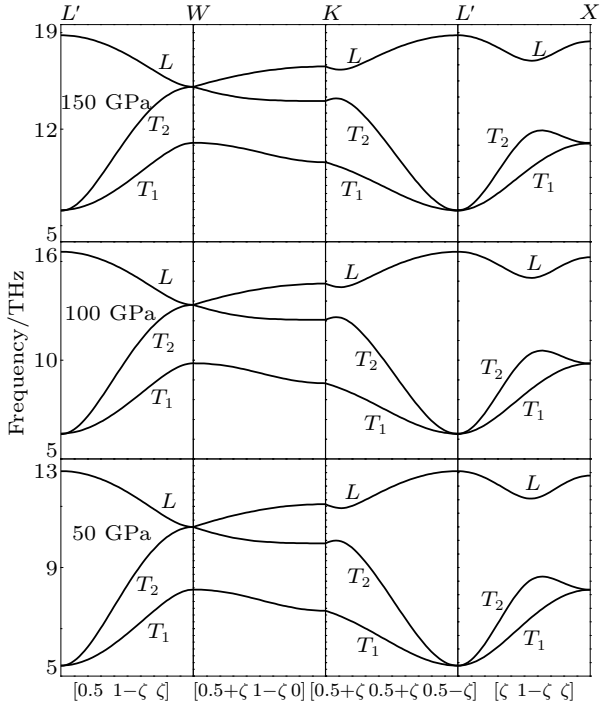


Fig. 6. Phonon dispersion curves of Cu along off-symmetry directions at different pressures.

In order to further illustrate the validity of phonon dispersion under high pressures, we use the obtained phonon dispersion relation as an essential input to calculate the values of specific heat (C_P) of Cu as a function of temperature at different pressures. $30 \times 30 \times 30$ Monkhorst–Pack mesh[30] are used in the calculations, and calculation details are given previously.[31,32] The calculated values of specific heat are plotted in Fig. 7. It can be seen that the calculated values of specific heat at zero pressure are in agreement with the experimental data given by Hultgern *et al*,[33] especially for the case of lower temperature. Like the result at zero pressure, the values of C_P increase with temperature at high pressures, and the value of C_P increases markedly with temperature below about 250 K, but it becomes almost constant at high temperatures. At the same temperature, the value of C_P decreases with increasing pressure. The phenomena were also observed in many previous investigations for some other metals under high pressures,[34–36] indicating that the MAEAM provides a reasonable description of lattice dynamics at high pressures.

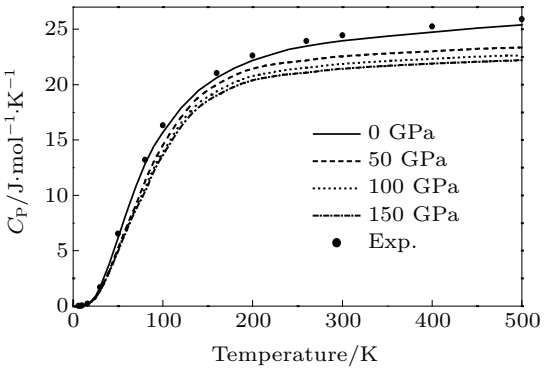


Fig. 7. Variations of specific heat C_P with temperature at different pressures.

4. Conclusions

In this paper, the MAEAM is used to reproduce the experimental results of the phonon dispersion in metal Cu at zero pressure along three high-symmetry directions and four off-symmetry directions by combining the theory of lattice dynamics. The phonon dispersion curves of Cu along all considered directions are simulated under high pressures of 50, 100, and 150 GPa. The results show that the vibration frequencies of Cu in all vibration branches at 50, 100, and 150 GPa are larger than that at zero pressure, and the frequencies increase correspondingly with pressure up to 50, 100, and 150 GPa, sequentially. Moreover, an anomalous dispersion is exhibited in the T_1 $[0\zeta\,\zeta]$ branch at high pressures. The simulated results along three symmetry directions at high pressures are consistent with the findings of other fcc metals when the differences in mass, interatomic spacing, and melting temperature among these metals are taken into account, suggesting that the modified analytic embedded atom method can be used to describe phonon dispersion relation at high pressures.

References

[1] Wang Y, Hector L G and Zhang H 2008 *Phys. Rev. B* **78** 104113
[2] Wang J F, Chen W Z and Jiang Z Y 2012 *Chin. Phys. B* **21** 077102
[3] Yang Y H, Dong S L and Wang L 2008 *Chin. Phys. B* **17** 270
[4] Shi L W, Duan Y F, Yang X Q and Tang G 2012 *Chin. Phys. Lett.* **28** 100503
[5] Ozisik H B, Colakoglu K and Deligoz E 2012 *Comput. Mater. Sci.* **51** 83
[6] Mittal R, Chaplot S L, Bose P P and Choudhury N 2007 *J. Phys.: Condens. Ser.* **92** 012143
[7] Sha X W and Cohen R E 2006 *Phys. Rev. B* **73** 104303
[8] Wortmanna G, Ponkratza U, Bielemeiera B and Rupprechtc K 2008 *High Press. Res.* **28** 545
[9] Wagner J M and Bechstedt F 2000 *Phys. Rev. B* **62** 4526
[10] Mujica A, Rubio A, Munoz A and Needs R J 2003 *Rev. Mod. Phys.* **75** 863
[11] Fang H, Liu B and Gua M 2010 *Physica B* **405** 732
[12] Hu C E, Zeng Z Y and Zhang L 2010 *J. Appl. Phys.* **107** 093509
[13] Dow M S and Baskes M I 1983 *Phys. Rev. Lett.* **50** 1285
[14] Dow M S and Baskes M I 1984 *Phys. Rev. B* **29** 6443

[15] Ouyang Y F, Zhang B W, Liao S Z and Jin Z P 1996 *Z. Phys. B* **101** 161
[16] Zhang B W, Ouyang Y F, Liao S Z and Jin Z P 1999 *Phys. B* **262** 218
[17] Xin H, Zhang J M, Wei X M and Xu K W 2005 *Surf. Interface Anal.* **37** 608
[18] Zhang J M, Wei X M and Xin H 2005 *Appl. Sur. Sci.* **243** 1
[19] Wen Y N and Zhang J M 2007 *Solid State Commun.* **144** 163
[20] Hu W Y, Shu X L and Zhang B W 2002 *Comput. Mater. Sci.* **23** 175
[21] Zhang J M, Song X L and Zhang X J 2006 *Surf. Sci.* **600** 1277
[22] Kazanc S, Ozgen S and Adiguzel O 2003 *Physica B* **334** 375
[23] Gurler Y and Ozgen S 2003 *Mater Lett.* **57** 4336
[24] Rose J H, Smith J R, Guinea F and Ferrante J 1984 *Phys. Rev. B* **29** 2963
[25] Vinet P, Rose J H, Ferrante J and Smith J R 1989 *J. Phys.: Condens. Matter* **1** 1941
[26] Dewaele A, Loubeyre P and Mezouar M 2004 *Phys. Rev. B* **70** 094112
[27] Zhang X J and Chen C L 2012 *J. Low Temp. Phys.* **169** 40
[28] Svensson E C, Vrockhouse B M and Rowe J M 1967 *Phys. Rev.* **155** 619
[29] Xie J J and Chen S P 2000 *Phys. Rev. B* **62** 3624
[30] Monkhorst H J 1976 *Phys. Rev. B* **13** 5188
[31] Chen H H, Li Z and Cheng Y 2011 *Physica B* **406** 3338
[32] Zhang D and Sun J X 2012 *Chin. Phys. B* **21** 080508
[33] Hultgern R, Orr R L and Anderson P D 1963 *Selected Values of Thermodynamic Properties of Metals and Alloys* (New York: Wiley)
[34] Zeng Z Y, Hu C E and Cai L C 2010 *J. Phys. Chem. B* **114** 298
[35] Umehara I, Hedo M and Tomioka F 2007 *J. Phys. Soc. Jpn.* **76** 206
[36] Aquino N 2009 *Rev. Mex. Fis.* **55** 125